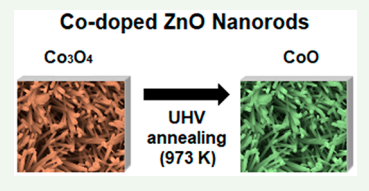
www.acsanm.org

Evolution of the Stoichiometry and Electronic Structure of Cobalt Oxide in Thermally Treated Co-Doped ZnO Nanorods for Solar Cells

Elena Echeverria, † Amrit Kaphle, † Aaron Austin, † Lyndon Bastatas, † Parameswar Hari, ‡, § and David Mcllroy*,†,§®

Supporting Information

ABSTRACT: The effects of annealing on the stoichiometry and electronic structure of Codoped ZnO nanorods (NRs), as prepared by chemical bath deposition (CBD), were investigated by photoemission spectroscopies (XPS and UPS) and X-ray diffraction (XRD). The Co 2p core level state of the as-grown Co-doped ZnO NRs is consistent with a Co₃O₄ stoichiometry, independent of the Co concentration. Upon annealing of the as-grown material above 865 K, a Co 2p core level satellite state forms, which is consistent with the formation of CoO. The valence band density of states also exhibits changes with annealing,



where a new density of states forms between the Fermi level and 1 eV below. The new valence band states are also consistent with the formation of CoO. This change in the cobalt oxide stoichiometry from Co₃O₄ to CoO results in Zn⁻ due to reduced O coordination, consistent with the Auger analysis. In addition, the evolution of Co₃O₄ to CoO is irreversible upon exposure to air. The oxidation state of Co is a key parameter in the material's performance when used for solar cells.

KEYWORDS: ZnO nanorods, Co-doped, DMS, photoemission spectroscopy, CoO, Co₃O₄

I. INTRODUCTION

The unique electrical and optical properties of ZnO make it a suitable material for a wide range of industrial applications in catalysis, photovoltaics, spintronics, and even gas sensors. 1-6 Of late, the dilute magnetic properties of transition-metal (TM)-doped ZnO suggest it may be a suitable material for use in spintronics, 7-10 where magnetically doped semiconductors are termed dilute magnetic semiconductors (DMS). Among the transition metals used to dope ZnO, cobalt (Co) and manganese (Mn) are the most common due to their high solubility limit compared to other metals. 8,9,11 The interest in DMS materials is due to the fact that both semiconducting and magnetic properties can simultaneously be controlled, which should allow for better control of spin transport in spin diodes and transistors. Furthermore, the Curie temperature on TMdoped ZnO-based DMSs is theoretically predicted to be above room temperature (RT). 5,12,13 Although some groups have observed ferromagnetism (FM) above RT in TM-doped ZnO, there are questions of reproducibility and if FM is an intrinsic effect. Furthermore, it has been shown that the preparation method and the form of the material (bulk, thin film, or nanostructured) play a role in their magnetic properties. Consequently, it is proposed that the defects and impurities associated with the method of preparation play a special role in the spintronic performance of devices constructed with them. 8,9,14,15

Along these lines, there is growing interest in understanding the behavior of nanoscale ZnO-based DMSs given that these nanostructures seem to be more stable and have high surfaceto-volume ratio, leading to enhancement in performance and interesting properties, as compared to thin films. In particular, it has been shown that ZnO nanorods (NRs) improve the absorption and sensitivity of ZnO gas sensors. 16 They are also good candidates for optoelectronics and energy conversion applications. 17,18 On other hand, Co inclusion has been shown to enhance the optical and magnetic properties of the ZnO NR. 19-23

Additionally, several experiments have demonstrated RT ferromagnetism of TM-doped ZnO nanostructures, 5,24-30 where ferromagnetism increases with annealing and is sensitive to the atmosphere in which samples are annealed. 5,28-30 However, if or why annealing of TM-doped ZnO nanostructures enhances their ferromagnetic properties is still an open question. Furthermore, studies of the effects of annealing on the stoichiometry of these nanostructures, in conjunction with their valence band electronic structure that will influence their magnetic properties, do not appear to have been conducted. Ghosh et al. have reported ferromagnetism at RT on CoO nanoparticles,³¹ and therefore the presence of CoO in Codoped ZnO nanostructures upon annealing could explain the ferromagnetic behavior, as opposed to attributing it to oxygen defects. \$5,29,30 The annealing environment obviously affects the oxidation state of the cobalt. For example, cobalt nitrite could form during annealing in N_2 , 26 as opposed to cobalt oxide in

Received: March 27, 2019 Accepted: June 21, 2019

Published: June 21, 2019



Department of Physics, Oklahoma State University, Stillwater, Oklahoma 74078-3072, United States

^{*}Department of Physics and Engineering Physics and *Oklahoma Photovoltaic Research Institute, University of Tulsa, Tulsa, Oklahoma 74104, United States

an O₂ atmosphere, ³²⁻³⁴ or reduction effects when samples are annealed in an ultrahigh vacuum (UHV).33

In this study, we explored the effects of UHV annealing on the stoichiometric and electronic properties of Co-doped ZnO NRs synthesized by a chemical bath deposition (CBD) method. We have developed a scalable, low-temperature chemical bath deposition method by which the morphology, doping levels, and aspect ratio of the nanostructures can be easily controlled. 19 We performed experiments on undoped ZnO NRs as well to differentiate between intrinsic effects of annealing and those associated with Co doping. Specifically, we studied the changes in electronic structures of these doped ZnO-based NRs as a function of Co content and annealing temperature using X-ray photoelectron spectroscopy (XPS), ultraviolet photoelectron spectroscopy (UPS), and X-ray diffraction (XRD).

II. EXPERIMENTAL SECTION

Cobalt-doped ZnO NRs were synthesized on Si substrates by the method of chemical bath deposition (CBD), described in detail in prior works³⁵ and illustrated in Figure 1. Briefly, ZnO nanorods

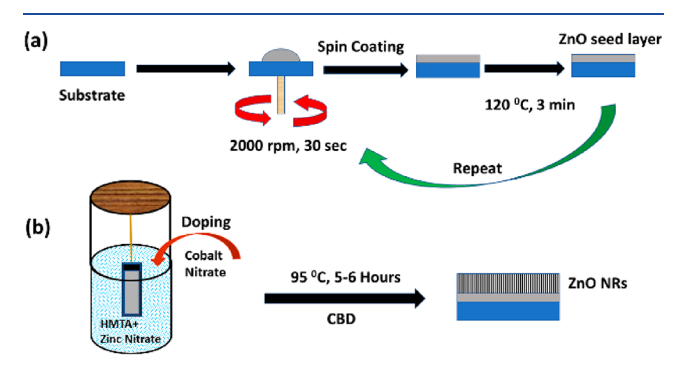


Figure 1. Schematic diagram of (a) ZnO seed layer fabrication method and (b) chemical bath deposition method for the growth of ZnO nanorods.

were grown with an equimolar (0.1 M) aqueous solution of zinc nitrate hexahydrate and hexamethylenetetramine. For cobalt-doped ZnO nanorods, cobalt nitrate hexahydrate was used as a doping agent with cobalt to a zinc molar percent of 5%, 10%, 15%, and 20%.

X-ray and ultraviolet photoelectron spectroscopies (XPS, and UPS) were performed at room temperature in a UHV chamber with a base pressure $< 10^{-9}$ Torr. The XPS spectra were acquired with the Al K α emission line from a dual-anode X-ray source (Physical Electronics XR 04-548) operated at 400 W, an incident angle of 54.7° and normal emission. UPS spectra were acquired by using both the He I (21.2 eV) and He II (40.8 eV) excitation lines from a UVS 40A2 UV source (PREVAC) at 54.7° and normal emission. While spectra were acquired with both UV photon energies, for brevity, only data with 21.2 eV photon energy are presented. The photoelectrons were collected and analyzed with an Omicrometer EA 125 hemispherical electron energy analyzer with a resolution of 0.02 eV. Samples were annealed between 773 and 973 K in vacuo by backside electron beam heating for 1 min, where the sample temperature was monitored with an infrared pyrometer (Marathon MA2SB). During the annealing process the pressure increased to $\sim 5 \times 10^{-8}$ Torr, and measurements were taken at least 1 h after the sample was annealed; this time was enough to allow the sample to cool to room temperature. XPS data were analyzed using the CasaXPS software package,³⁹ and a Shirley background was used and subtracted from the core level spectra presented herein.41,42

Crystal structures of undoped and doped ZnO NRs were determined using a Ricaku X-ray diffraction spectrometer (Cu Kα radiation, $\lambda = 1.54056$ Å). Rietveld refinement were performed using Rigaku PDXL XRD analysis software.

III. RESULTS

Displayed in Figure S1 (Supporting Information) are scanning electron microscopy (SEM) images of undoped and 15% cobalt-doped ZnO NRs. The hexagonal shape of the NRs is clearly seen for both undoped and doped samples. As expected, the Co-doped NRs have a larger diameter and are longer than the undoped ZnO-based NRs;³⁹ however, little is known whether these morphological changes impact the stoichiometry and/or electronic structure. Therefore, the aim of this work is to examine the oxidation states of the Zn and Co cations as a function of the Co concentration and their evolution with annealing. Results of the XPS and UPS studies are presented first, followed by the XRD study.

A. X-ray Photoelectron Spectroscopy Analysis. Displayed in Figure 2a are the XPS spectra of the Zn 2p core level

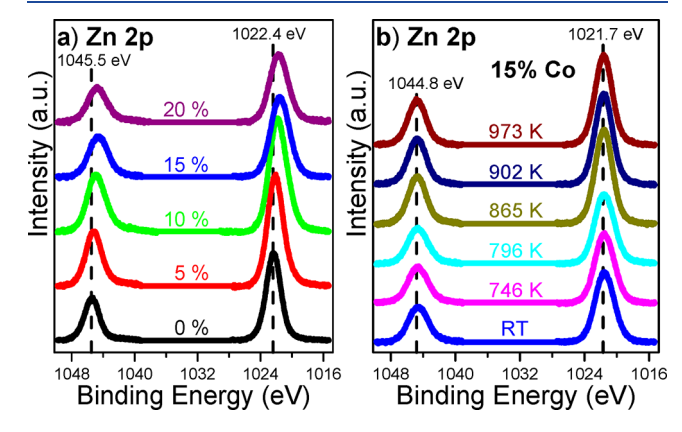


Figure 2. XPS core level spectra of the Zn 2p of ZnO NRs (a) asgrown samples as a function of Co content and (b) annealing dependence for the 15% Co-doped sample.

states as a function of Co doping. The binding energies of the Zn $2p_{3/2}$ and $2p_{1/2}$ peaks are 1022.4 and 1045.5 eV, respectively, with a spin-orbital splitting of 22.9 eV, in agreement with previously reported values. 6,43,44 The Zn 2p core level steadily shifts to lower binding energy with increasing Co doping, where the maximum shift of 0.85 eV occurs for 15% Co. However, it shifts back 0.2 eV to higher binding energy for 20% Co. Furthermore, the full width at halfmaximum (fwhm) of the Zn 2p core level state increases from 2.19 eV for undoped ZnO to 2.80 eV for 20% Co content. The core level shift is consistent with the formation of metallic-like Zn bonds. 6,45 However, the increase in the fwhm suggests either of two things: the ZnO lattice becomes more disordered with increasing Co concentration, where disorder is due to defects in the form of interstitials, substitution, oxygen vacancy defects, and so on, 7,29 or the coexistence of zinc oxide and cobalt oxide regions within the ZnO NRs. If we assume the latter, the lower binding energy of the Zn 2p with Co doping is due to a higher content of Zn cations with fractionally more negative charge, where the formation of cobalt oxides scavenges oxygen from the zinc oxide. Furthermore, at 20% Co content, there exists regions of ZnO with 10% Co content (higher Zn 2p binding energy) and regions with clusters of cobalt oxide (lower Zn 2p binding energy), where this is based on the comparison with the spectrum for 10% Co doping. This

suggests that clustering of cobalt oxide occurs at 15% Co doping.

Figure 2b shows the annealing dependence of the Zn 2p core level of the 15% Co-doped sample. The binding energies of the Zn 2p peaks and the oxidation state remain unchanged with annealing, regardless of Co content. However, with annealing, the fwhm of the Zn 2p core level state for 20% Co-doped sample decreases from 2.80 to 2.17 eV, indicative of improved short-range order.

Zn LMM Auger spectra were also collected for additional information about the ZnO stoichiometry with Co doping. A comparison of the Auger spectra of the as-grown 0% and 15% Co samples are presented in Figure 3a. The predominant

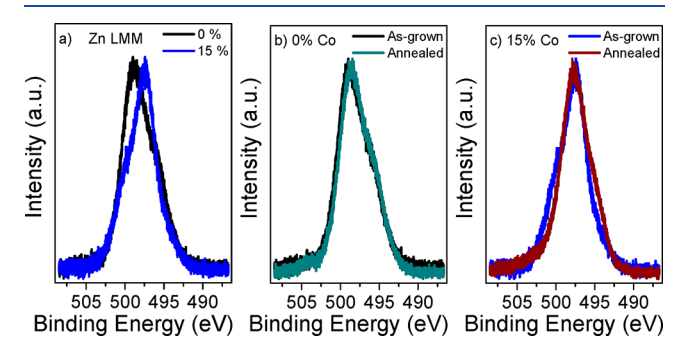


Figure 3. Zn LMM Auger peak of (a) the as-grown undoped ZnO NRs (black line) and the as-grown 15% Co-doped NRs (blue line), (b) as-grown (black) and annealed (cyan) undoped ZnO NRs, and (c) as-grown (blue) and annealed (purple) 15% Co-doped ZnO NRs.

weighting of the Zn LMM Auger peak of the 15% Co-doped sample is on the lower binding energy, in contrast to the undoped sample, and is indicative of less positive Zn cations. It has been proposed that Co doping results in metallic Zn, 6,46 but we believe the correct identification is $\mathrm{Zn}^{+2-\delta}$, where $0 < \delta < 1$, and is associated with nonstoichiometric ZnO. Our conclusion is supported by the corresponding valence band spectra, presented below. Upon annealing of the 15% Co sample, the leading edge of the Zn LMM Auger spectrum shifts to lower binding energy, where spectral weight is transferred from the trailing edge to the leading edge (Figure 3c). In contrast, the Auger spectrum of the undoped ZnO sample is unchanged with annealing (Figure 3b), confirming that any change on the stoichiometric of Zn is due to the presence of

Spectra of the Co 2p core level states as a function of Co concentration are displayed in Figure 4a, where the relative intensity of the Co signal increases with Co concentration. On the basis of the binding energy of the Co $2p_{3/2}$ and $2p_{1/2}$ core level states of 780 and 795 eV and the absence of shakeup satellite features at 786 and 803 eV of the as-grown samples, regardless of Co concentration, we conclude that Co₃O₄ is preferentially formed over CoO.^{9,24,34,47–49} Note that the binding energies of the Co 2p core level states do not shift with increasing Co concentration. However, upon annealing, the line shapes of the Co 2p core levels, regardless of Co concentration, become more asymmetric, and shakeup satellite peaks emerge. The evolution of the Co 2p core level state for 15% Co as a function of annealing temperature is presented in Figure 4b and is typical for all levels of doping in this study. The broadening of the Co 2p core level states and the emergence of the shakeup satellite peaks at 785.9 and 802.9 eV are indicative of the evolution from Co₃O₄ to CoO or from the

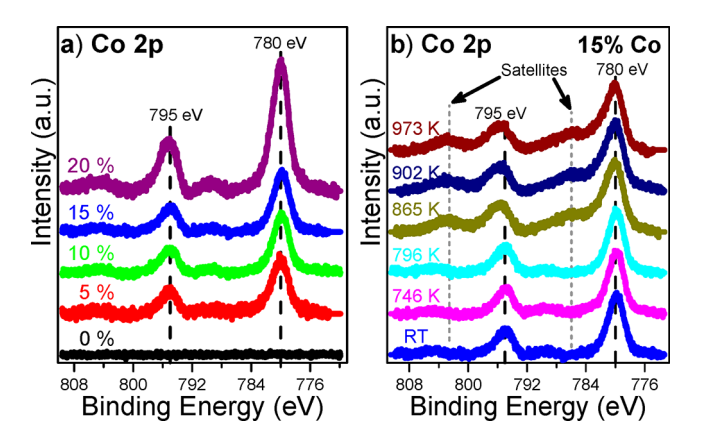


Figure 4. XPS core level spectra of the Co 2p of ZnO NRs of (a) asgrown samples as a function of Co content and (b) annealing dependence for the 15% Co-doped sample.

mixed oxidation state Co²⁺ and Co³⁺ to purely Co²⁺, respectively.^{19,47} The change in the stoichiometry of cobalt oxide with annealing is significant, as the oxidation state of Co plays an important role in the performance of the material in catalytic and photovoltaic applications.^{3,32}

The O 1s core level state of the as-grown Co-doped ZnO NRs as a function of Co concentration are displayed in Figure S2a. The O 1s binding energy of undoped ZnO is 531 eV. Upon doping with Co, a new, low binding energy, oxygen state is observed at 529.8 eV that increases in intensity with increasing Co concentration and corresponds to either Co₃O₄, CoO, or a mixture thereof. Both forms of cobalt oxide have spectral weights at 531 and 529.8 eV. Displayed in Figure S2b are O 1s core level spectra of ZnO NRs with 15% Co as a function of annealing and are representative of all of the Co concentrations in this study. Although not shown here, the O 1s spectra of the undoped sample became gradually sharper upon annealing; therefore, the main peak at 531 eV for all the samples is assigned to O²⁻ ions in the ZnO wurtzite structure.

Upon annealing, the O 1s core level state at 531 eV of all the Co-doped samples shows a significant loss in spectral weight, while the peak at 529.8 eV becomes sharper. Even though this peak does not prove the formation of CoO, it is an indication that at the surface there is more contribution of states related to cobalt rather than from zinc.

B. Ultraviolet Photoelectron Spectroscopy Analysis. Displayed in Figure 5a are the valence band (VB) spectra of asgrown Co-doped ZnO NRs as a function of Co concentration, and in Figure 5b are their postannealed VB spectra. The VB spectrum of the undoped as-grown sample (0% in Figure 5a) is composed of two main bands, where the one centered around 11 eV corresponding to Zn 3d states and the broad band from 5 to 7 eV is assigned to O 2p states. With the incorporation of Co, a band emerges at ~1.5 eV that shifts and grows in intensity with increasing Co concentration. This is the Co 3d band of cobalt oxide^{51°} and is likely hybridized with Zn 4s orbitals.⁵² Upon annealing the as-grown samples, the characteristic Zn 3d and O 2p states become more pronounced and well-defined, indicative of improved ordering of the ZnO lattice, i.e., healing of defects, etc. Additionally, the establishment of the density of states (DOS) very close to the Fermi level $(E_{\rm F})$ is observed for samples with high Co content (\geq 15%). These new DOS correspond to the formation of CoO, 45-47 in agreement with the XPS results herein.

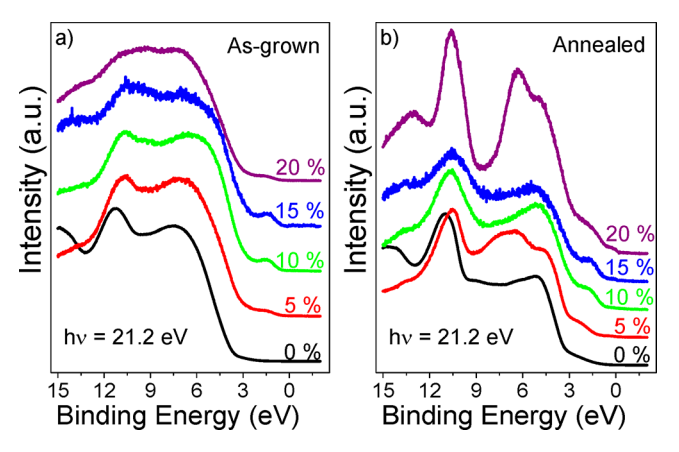


Figure 5. Valence band spectra for ZnO NRs samples (a) as-grown and (b) after annealing at the maximum temperature.

Displayed in Figure 6 are UPS spectra of the region near the $E_{\rm F}$ as a function of annealing temperature of undoped and 15%

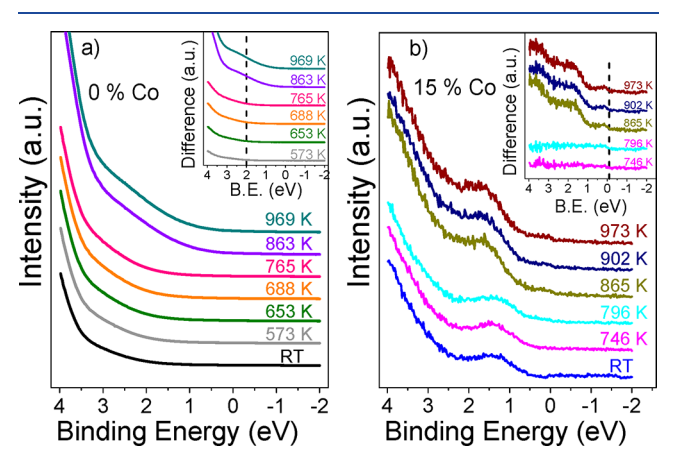


Figure 6. Valence band spectra of undoped (a) and 15% Co-doped (b) ZnO NRs as a function of annealing temperature, where $h\nu=21.2$ eV. The insets are difference spectra with respect to spectrum of the as-prepared, undoped, ZnO NRs sample.

Co content ZnO NRs samples. In the case of the undoped ZnO NRs sample, the DOS in the vicinity of $E_{\rm F}$ (see the inset in Figure 6a) is unchanged. However, for 15% Co-doped ZnO NRs annealed to ~750 K, a new DOS emerges in the vicinity of $E_{\rm F}$ (see the inset in Figure 6b), which is characteristic of CoO formation. ^{47,49}

The integrated density of states (I-DOS) of the UPS spectra from -2 to 4 eV of the as-grown Co-doped samples and after annealing at the maximum temperature are plotted in Figure 7. From inspection of Figure 7, it is apparent that the I-DOS is much higher upon annealing, regardless of doping, but increase significantly with Co doping. The rapid rise in the I-DOS is due to the evolution of Co_3O_4 to CoO and discussed in section IV.

C. X-ray Diffraction Analysis. Figure S3 shows the XRD patterns of 0%–20% cobalt-doped ZnO NRs and corresponding Rietveld analysis. For undoped and 5% cobalt-doped samples (Figure S3a,b), all the XRD diffraction peaks are well matched to the ZnO wurtzite-phase structure (JCPDS No. 36-1451). This indicates that the Co²⁺ ions are well-substituted into Zn sites during doping without the creation of a secondary phase, at least within the detection limits. All the undoped and

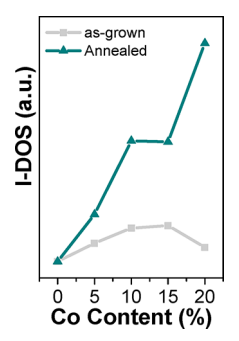


Figure 7. Integrated valence band spectra from -2 to 3.76 eV as a function of Co doping for the as-grown samples (gray squares) and after annealing at the maximum temperature (cyan triangles).

cobalt doped ZnO are highly c-axis oriented, where the (002) diffraction peak position gradually shifts toward smaller angles with higher cobalt doping. For 10%, 15%, and 20% cobalt doping (Figure S3c-e), we observe an additional spinel ZnCo₂O₄ phase, which is a typically observed spinel structure with Zn²⁺ ions in the tetrahedral sites and Co³⁺ occupying the octahedral sites. Rietveld analysis of these samples (10%–20%) revealed that the percentage of ZnO phase in samples decreases and the secondary phase of ZnCo₂O₄ increases with increasing cobalt concentration. The results of Rietveld analysis are summarized in Table S1.

The lattice parameter c increases from 5.2061 to 5.2084 Å, and a varied from 3.2500 to 3.2514 Å with increasing cobalt concentration, as shown in Table S1. The expansion of the unit cell in the c-axis direction produces distortions in the unit cell and leads to compressive stress in ZnO nanorods. ⁵⁴ Because of the mismatch between the ionic radii of Zn²⁺ and Co²⁺, the crystallite size increases from 50.022 to 73.232 nm. As a result, the presence of interstitial atoms at higher cobalt concentrations increases the lattice volume, thereby increasing the average crystal size. ⁵⁵

Figure S4 shows the XRD analysis of 15% cobalt-doped samples treated at 773 K (Figure S4a), 873 K (Figure S4b), and 973 K (Figure S4c). One sees that the intensity of ZnO peaks gradually increases with temperature, indicating an increased release of zinc from the spinel structure. This is attributed to the energetic advantage of placing the d⁶ ions in octahedral sites, where adoption of the low-spin configuration gives it a decisively favorable crystal field stabilization energy. Accordingly, the ionic radii of the cationic species in this spinel structure are 0.60 and 0.55 Å for the Zn²⁺ and Co³⁺ ions, respectively.⁵⁸ When the temperature is increased to 873 K, Co³⁺ starts to reduce to Co²⁺; as a result, a mixture of both Co₃O₄ (5.13%) and CoO (6.91%) phases are present. As the reduction of Co³⁺ ions progresses, more and more zinc is released, subsequently leading to a more cobalt-enriched spinel. However, in the case where all of the cobalt is present as Co²⁺, the absence of trivalent ions will lead to the collapse of the spinel structure, and a mixture of ZnO and only CoO can thus be expected.⁴ Note that the sample annealed at 973 K has small traces of Co₃O₄ (2.43%) present. This indicates that Co₃O₄ is not fully converted into CoO. Consequently, in the annealing temperature range between 873 and 973 K, the three components ZnO, spinel Co₃O₄, and rock-salt CoO coexist. With annealing above 973 K, Co³⁺ starts to reduce to Co²⁺, and these ions can substitute for the Zn2+ ions in the tetrahedral positions of the spinel arrangement. In this way,

zinc is released from the spinel structure, leading to ZnO and a cobalt-enriched spinel. 50

IV. DISCUSSION

Typically, the CoO (Co²⁺) phase is observed for Co-doped ZnO films, 6,9,15,59 yet XPS measurements of the Co 2p core level state of Co-doped nanostructures reveal the presence of Co^{2+} and Co^{3+} or only Co^{2+} , corresponding to either $Co_3O_4^{60-62}$ or $CoO_7^{27,63-66}$ where the speciation depends on the method of materials preparation. The Co 2p XPS spectra in Figure 4a of as-prepared Co-doped ZnO NRs synthesized by CBD clearly indicate the presence of the Co₃O₄ phase; however, Figure 4b shows that CoO phase can be obtained by annealing the samples under UHV conditions. Annealing affects not only the oxidation state of the cobalt but also that of the Zn present in the samples, as evident in the Zn LMM Auger spectra (Figure 3). The changes in the Zn Auger spectra indicate that zinc goes from Zn^{2+} to $Zn^{+2-\delta}$, where $0 < \infty$ δ < 1, in doped samples when annealed at high temperatures in

The annealing of the samples in UHV has the same effect as the reducing process shown in eq 1.33

$$2\text{Co}_3\text{O}_4 \to 6\text{CoO} + \text{O}_2 \tag{1}$$

Therefore, the UHV annealing of samples containing Co₃O₄ will lead to CoO formation as well as oxygen vacancies. The loss of oxygen is verified by the decrease in atomic concentration obtained by the XPS analysis in Figure 8a.

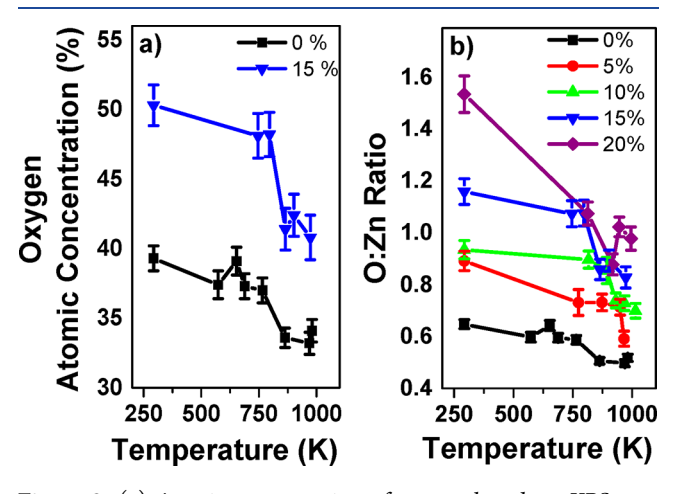


Figure 8. (a) Atomic concentration of oxygen based on XPS as a function of temperature for the undoped sample (black squares) and 15% Co (blue triangles). (b) O:Zn ratio for undoped and Co-doped samples as a function of annealing temperature.

The loss of O associated with ZnO coincides with the formation of the CoO phase; i.e., O is scavenged by Co to transform Co₃O₄ to CoO. Although there is also a decrease in the oxygen content for the undoped sample, it is attributed to elimination of oxygen impurities on the ZnO surface and the healing of defects.⁶⁷ Reduction of ZnO requires high temperatures on the order of 1000 K.68 Additionally, the oxygen-to-zinc ratio (O:Zn) shows a more pronounced change in samples containing Co relative to the undoped sample, as shown in Figure 8b.

In addition to the verification of the CoO phase of cobalt oxide by photoelectron spectroscopy (XPS and UPS) and Xray diffraction, visual inspection before and after annealing

revealed that the color of the 15% Co-doped ZnO NR sample changed from brownish to greenish when heated at high temperatures. To evaluate the stability of the CoO surface layer, the samples were removed from the UHV chamber and exposed to ambient laboratory conditions for several months and then returned to the UHV chamber for XPS characterization. The XPS analysis revealed some oxygen contamination on the surface, but the oxidation state of Co remained CoO. Therefore, the presence of CoO in these samples is stable at ambient temperature and atmospheric conditions and needs to be annealed in O₂ to transform CoO back to Co₃O₄.³

The change in the stoichiometry of cobalt in heavily doped ZnO presented here indicates that it should be accounted for when the material is used in a vacuum or reducing environments. For example, in CO conversion processes, the oxidation state of the metal catalyst is critical to the reaction process given that in some reactions the presence of CoO is more effective catalyst than those containing Co₃O₄.33 Additionally, the photocatalytic efficiency of a catalyst containing cobalt relies on the competition between Co²⁺ and Co3+ ions and the band gap of the material.62 The UPS measurements herein have shown that the formation of a CoO phase is accompanied by new DOS in the vicinity of $E_{\rm F}$, and as a result, the band gap of these samples decreases. Therefore, the evolution of Co₃O₄ to CoO in heavily doped ZnO should be accounted for when interpreting its impact on materials properties and performances of devices.

Additionally, the impact of our findings may be relevant to the ongoing debate concerning the room temperature ferromagnetism (FM) of Co-doped ZnO. Three main arguments have been proposed to explain the observed FM: (i) proper substitution of Co cations within the host lattice, ^{17,27,28,49,69,70} (ii) O vacancies and defects associated with ZnO, ^{7,14,24,27,28,52,59,60,71} and (iii) Co clustering or second phases. 72,73 We postulate the unintended formation of the CoO phase cobalt oxide in Co-doped ZnO may account for the ferromagnetic properties, which have inadvertently attributed to O vacancies and defects. It has been proposed that Co doping of ZnO introduces Co²⁺ ions that produce a red-shift of the optical absorption band, increases sp-d exchange interactions and activates d-d transitions, but without changing the ZnO wurtzite structure. 69 The observed FM may arise from CoO on the surface of the ZnO NRs and in contact with the subsurface Co₃O₄, i.e., the formation of a Co₃O₄/CoO interface, as revealed in the X-ray diffraction analysis, which increases the concentration of Co²⁺ ions and shifts the band edge (see UPS data in Figure 6b), in agreement with prior studies. 66,69,74,75 Lim et al. 69 ruled out CoO as the source of FM because it is antiferromagnetic and instead suggested that Co clusters exist within the ZnO.⁶⁹ This study found no evidence to support Co cluster formation. We speculate that strained CoO at the surface or within clusters of CoO may be responsible for the reported FM.66 We cannot rule out the oxygen vacancies (Vo) as source of FM, but we attribute it as a consequence of Co-V_o interactions rather than just V_o, as mentioned in refs 76 and 77. While this study does not address room temperature FM of Co-doped ZnO, it brings to light new information about the evolution of the oxidation state of Co and that the presence of CoO in heavily Co-doped ZnO, which is important to understand the materials room temperature FM. Furthermore, the inconsistency of the reports of room temperature FM of Co-doped ZnO may be due to the lack of reproducibility of the initial oxidation state of Co. For

example, if Co₃O₄ is the predominant oxide phase in Co-doped ZnO, the reduction process will lead to CoO formation and oxygen vacancies within the ZnO phase, concomitant with the emergence of room temperature FM. Alternatively, if CoO is the predominant oxide phase in the as-grown material, annealing in UHV or a mild reducing atmosphere will not affect the CoO phase or increase the density of oxygen vacancies within the ZnO.

V. CONCLUSION

In conclusion, we have explored the effects of annealing in vacuo on the stoichiometry of Co-doped ZnO-based nanorods prepared by chemical bath deposition. X-ray photoelectron spectroscopy showed that the inclusion of Co causes the Zn 2p core level to shift to lower binding energy relative to the undoped material, indicative of the reduction in its ionicity. XPS, UPS, and XRD measurements showed that the stoichiometry of the cobalt oxide of the as-prepared samples is Co₃O₄ and independent of the Co concentration. The stoichiometric state of Zn was unaffected by UHV annealing. In contrast, the oxidation state of cobalt changed from Co₃O₄ to CoO with UHV annealing, in concert with an increase in the density of oxygen vacancies. Cobalt in the form of CoO increases the density of divalent cations relative to Co₃O₄ and, therefore, may be responsible for the reported room temperature ferromagnetism of Co-doped ZnO with annealing. Additionally, the results presented herein are important to catalytic and photovoltaic applications of Co-doped ZnO since their performance depends on the oxidation state of the dopant metals.

ASSOCIATED CONTENT

Supporting Information

The Supporting Information is available free of charge on the ACS Publications website at DOI: 10.1021/acsanm.9b00574.

Scanning electron microscope images, XPS spectra of the O 1s core level, XRD patterns of 0%-20% cobaltdoped ZnO NRs and annealed 15% Co-doped, Rietveld summary table analysis (PDF)

AUTHOR INFORMATION

Corresponding Author

*E-mail dave.mcilroy@okstate.edu.

ORCID ®

Elena Echeverria: 0000-0002-9472-6288 Lyndon Bastatas: 0000-0003-1199-9676 David Mcllroy: 0000-0001-9438-3775

The authors declare no competing financial interest.

ACKNOWLEDGMENTS

We acknowledge Oklahoma NASA EPSCoR (NNX13AN01A and NNX15AM75A) for financial support. OSU acknowledges the support of the Office of Naval Research (N00014-17-1-2593). D.M. acknowledges B. Love for useful discussions about this work.

ABBREVIATIONS

NRs, nanorods; CBD, chemical bath deposition; XPS, X-ray photoemission spectroscopy; UPS, ultraviolet photoemission spectroscopy; TM, transition metal; DMS, diluted magnetic semiconductors; RT, room temperature; FM, ferromagnetism; UHV, ultrahigh vacuum; SEM, scanning electron microscopy; fwhm, full width at half-maximum; VB, valence band; DOS, density of states; I-DOS, integrated density of states; $E_{\rm E}$, Fermi level; V_o, oxygen vacancies.

REFERENCES

- (1) He, R.; Hocking, R. K.; Tsuzuki, T. Co-doped ZnO Nanopowders: Location of Cobalt and Reduction in Photocatalytic Activity. Mater. Chem. Phys. 2012, 132, 1035-1040.
- (2) Ruckh, M.; Schmid, D.; Schock, H. W. Photoemission Studies of the ZnO/CdS Interface. J. Appl. Phys. 1994, 76, 5945-5948.
- (3) Kim, T. W.; Woo, M. A.; Regis, M.; Choi, K.-S. Electrochemical Synthesis of Spinel Type ZnCo₂O₄ Electrodes for Use as Oxygen Evolution Reaction Catalysts. J. Phys. Chem. Lett. 2014, 5, 2370-
- (4) Klingshirn, C. ZnO: Material, Physics and Applications. ChemPhysChem 2007, 8, 782-803.
- (5) Djerdj, I.; Jagličić, Z.; et al. Co-Doped ZnO Nanoparticles: Minireview. Nanoscale. 2010, 2, 1096-1104.
- (6) Sulciute, A.; Baltrusaitis, J.; Valatka, E. Structure, Morphology and Electrochemical Properties of Zinc-Cobalt oxide Films on AISI 304 Type Steel. J. Appl. Electrochem. 2015, 45, 405-417.
- (7) Lee, H.-J.; Jeong, S.-Y.; Cho, C. R.; Park, C. H. Study of Diluted Magnetic Semiconductor: Co-Doped ZnO. Appl. Phys. Lett. 2002, 81, 4020-4022.
- (8) Kittilstved, K. R.; Liu, W. K.; Gamelin, D. R. Electronic structure Origins of Polarity-Dependent High-TC Ferromagnetism in Oxide-Diluted Magnetic Semiconductors. Nat. Mater. 2006, 5, 291-297.
- (9) Wei, L.; Li, Z.; Zhang, W. F. Influence of Co Doping Content on Its Valence State in $Zn_{1-x}Co_xO$ ($0 \le x \le 0.15$) Thin Films. *Appl. Surf.* Sci. 2009, 255, 4992-4995.
- (10) Liu, W. K.; Whitaker, K. M.; Kittilstved, K. R.; Gamelin, D. R. Stable Photogenerated Carriers in Magnetic Semiconductor Nanocrystals. J. Am. Chem. Soc. 2006, 128, 3910-3911.
- (11) Mizokawa, T.; Nambu, T.; Fujimori, A.; Fukumura, T.; Kawasaki, M. Electronic Structure of the Oxide-Diluted Magnetic Semiconductor $Zn_{1-x}Mn_xO$. *Phys. Rev. B: Condens. Matter Mater. Phys.* 2002, 65, 085209.
- (12) Dietl, T.; Ohno, H.; Matsukura, F.; Cibert, J.; Ferrand, D. Zener Model Description of Ferromagnetism in Zinc-Blende Magnetic Semiconductors. Science 2000, 287, 1019-1022.
- (13) Sato, K.; Katayama-Yoshida, H. First Principles Materials Design for Semiconductor Spintronics. Semicond. Sci. Technol. 2002, 17, 367-376.
- (14) Venkatesan, M.; Fitzgerald, C. B.; Lunney, J. G.; Coey, J. M. D. Anisotropic Ferromagnetism in Substituted Zinc Oxide. Phys. Rev. Lett. 2004, 93, 177206.
- (15) El Manouni, A.; Tortosa, M.; Manjón, F. J.; Mollar, M.; Marí, B.; Sánchez-Royo, J. F. Effect of Annealing on Zn_{1-x}Co_xO Thin Films Prepared by Electrodeposition. Microelectron. J. 2009, 40, 268-271.
- (16) Wang, J. X.; Sun, X. W.; Yang, Y.; Huang, H.; Lee, Y. C.; Tan, O. K.; Vayssieres, L. Hydrothermally Grown Oriented ZnO Nanorod Arrays for Gas Sensing Applications. Nanotechnology 2006, 17, 4995-
- (17) Shatnawi, M.; Alsmadi, A. M.; Bsoul, I.; Salameh, B.; Alna'washi, G. A.; Al-Dweri, F.; El Akkad, F. Magnetic and Optical Properties of Co-Doped ZnO Nanocrystalline Particles. J. Alloys Compd. 2016, 655, 244-252.
- (18) Park, J.-W.; Park, C.-M. Mechanochemically Induced Transformation of CoO(OH) Into Co₃O₄ Nanoparticles and Their Highly Reversible Li Storage Characteristics. RSC Adv. 2017, 7, 10618-
- (19) Kaphle, A.; Reed, T.; Apblett, A.; Hari, P. Doping Efficiency in Cobalt-Doped ZnO Nanostructured Materials. J. Nanomater. 2019,
- (20) Kuriakose, S.; Satpati, B.; Mohapatra, S. Enhanced Photocatalytic Activity of Co Doped ZnO Nanodisks and Nanorods

- Prepared by Facile Wet Chemical Method. Phys. Chem. Chem. Phys. 2014, 16, 12741–12749.
- (21) Chanda, A.; Gupta, S.; Vasundhara, M.; Joshi, S. R.; Mutta, G. R.; Singh, J. Study of Structural, Optical and Magnetic Properties of Doped ZnO Nanorods. *RSC Adv.* **2017**, *7*, 50527.
- (22) Hammad, T. M.; Salem, J. K.; Harrison, R. G. Structure, Optical Properties and Synthesis of Co-Doped ZnO Superstructures. *Appl. Nanosci.* **2013**, *3*, 133–139.
- (23) Kuriakose, S.; Satpati, B.; Mohapatra, S. Facile Synthesis of Co Doped ZnO Nanodisks for Highly Efficient Photocatalytic Degradation of Methyl Orange. *Adv. Mater. Lett.* **2015**, 6 (3), 217–223.
- (24) Wang, X. F.; Xu, J.; Zhang, B.; Yu, H.; Wang, J.; Zhang, X.; Yu, J.; Li, Q. Signature of Intrinsic High-Temperature Ferromagnetism in Cobalt-Doped Zinc Oxide Nanocrystals. *Adv. Mater.* **2006**, *18*, 2476–2480
- (25) Wang, H. B.; Wang, H.; Zhang, C.; Yang, F. J.; Yang, C. P.; Gu, H. S.; Zhou, M. J.; Li, Q.; Jiang, Y. Effect of Annealing on the Magnetic Properties of Solution Synthesized Zn_{1-x}Mn_xO Nanorods. *Mater. Chem. Phys.* **2009**, *113*, 884–888.
- (26) Rubi, D.; Fontcuberta, J.; Calleja, A.; Aragonès, L.; Capdevila, X. G.; Segarra, M. Reversible Ferromagnetic Switching in ZnO:(Co, Mn) Powders. *Phys. Rev. B: Condens. Matter Mater. Phys.* **2007**, 75, 155322.
- (27) Wang, H.; Wang, H. B.; Yang, F. J.; Chen, Y.; Zhang, C.; Yang, C. P.; Li, Q.; Wong, S. P. Structure and Magnetic Properties of $Zn_{1-x}Co_xO$ Single-Crystalline Nanorods Synthesized by a Wet Chemical Method. *Nanotechnology* **2006**, *17*, 4312–4316.
- (28) Zhou, X.; Ge, S.; Yao, D.; Zuo, Y.; Xiao, Y. Effect of Thermal Treatment on Room-Temperature Ferromagnetism in Co-Doped ZnO Powders. *Phys. B* **2008**, *403*, 3336–3339.
- (29) Pal, B.; Giri, P. K. High Temperature Ferromagnetism and Optical Properties of Co Doped ZnO Nanoparticles. *J. Appl. Phys.* **2010**, *108*, 084322.
- (30) Naeem, M.; Hasanain, S. K.; Mumtaz, A. Electrical Transport and Optical Studies of Ferromagnetic Cobalt Doped ZnO Nanoparticles Exhibiting a Metal–Insulator Transition. *J. Phys.: Condens. Matter* **2008**, 20, 025210.
- (31) Ghosh, M.; Sampathkumaran, E. V.; Rao, C. N. R. Synthesis and Magnetic Properties of CoO Nanoparticles. *Chem. Mater.* **2005**, 17, 2348–2352.
- (32) Petitto, S. C.; Marsh, E. M.; Carson, G. A.; Langell, M. A. Cobalt Oxide Surface Chemistry: The Interaction of CoO(100), Co₃O₄(110) and Co₃O₄(111) With Oxygen and Water. *J. Mol. Catal. A: Chem.* **2008**, *281*, 49–58.
- (33) Lin, H.-K.; Chiu, H.-C.; Tsai, H.-C.; Chien, S.-H.; Wang, C.-B. Synthesis, Characterization and Catalytic Oxidation of Carbon Monoxide over Cobalt Oxide. *Catal. Lett.* **2003**, *88*, 169–174.
- (34) Barreca, D.; Massignan, C.; Daolio, S.; Fabrizio, M.; Piccirillo, C.; Armelao, L.; Tondello, E. Composition and Microstructure of Cobalt Oxide Thin Films Obtained from a Novel Cobalt(II) Precursor by Chemical Vapor Deposition. *Chem. Mater.* **2001**, *13*, 588–593.
- (35) Kaphle, A.; Hari, P. Variation of Index of Refraction in Cobalt Doped ZnO Nanostructures. *J. Appl. Phys.* **2017**, *122*, 165304.
- (36) Hari, P.; Kaphle, A. Investigations on Cobalt Doped Nanostructured ZnO/p-Si Heterojunctions for Energy Conversion Devices; Nanomaterials and Nanotechnology Chapter: 4; One Central Press (OCP): 2016.
- (37) Kaphle, A.; Hari, P. Characterization of Aluminum Doped Nanostructured ZnO/p-Si Heterojunctions. *Int. J. Eng. Sci. IJES* **2016**, *5*, 41–51.
- (38) Farmer, K.; Hari, P.; Roberts, K. pH Study of Zinc Oxide Nanorods Grown on Indium Tin Oxide Coated Substrate. *Can. J. Phys.* **2014**, 92, 838–841.
- (39) Kaphle, A.; Echeverria, E.; Mcllroy, D. N.; Roberts, K.; Hari, P. Thermo-Optical Properties of Cobalt-Doped Zinc Oxide (ZnO) Nanorods. J. Nanosci. Nanotechnol. 2019, 19, 3893–3904.
- (40) Fairly, N. CasaXPS: Processing Software for XPS, AES, SIMS and More.

- (41) Colón Santana, J. A. Quantitative Core Level Photoelectron Spectroscopy: A Primer; Morgan and Claypool: San Rafael, CA, 2015.
- (42) Vegh, J. The Shirley background revised. J. Electron Spectrosc. Relat. Phenom. 2006, 151, 159-164.
- (43) Moulder, J. F.; Stickle, W. F.; Sobol, P. E.; Bomben, K. D. *Handbook of X-ray Photoelectron Spectroscopy; Jill Chastain*; Perkin-Elmer Corp.: Eden Prairie, MN, 1992.
- (44) Biesinger, M. C.; Lau, L. W. M.; Gerson, A. R.; Smart, R. S. C. Resolving Surface Chemical States in XPS Analysis of First Row Transition Metals, Oxides and Hydroxides: Sc, Ti, V, Cu and Zn. Appl. Surf. Sci. 2010, 257, 887–898.
- (45) Deroubaix, G.; Marcus, P. X-ray Photoelectron Spectroscopy Analysis of Copper and Zinc Oxides and Sulphides. *Surf. Interface Anal.* **1992**, *18*, 39–46.
- (46) Zhang, Y.; Du, G.; Wang, X.; Li, W.; Yang, X.; Ma, Y.; Zhao, B.; Yang, H.; Liu, D.; Yang, S. X-ray Photoelectron Spectroscopy study of ZnO Films Grown by Metal-Organic Chemical Vapor Deposition. *J. Cryst. Growth* **2003**, 252, 180–183.
- (47) Shen, Z.-X.; Allen, J. W.; Lindberg, P. A. P.; Dessau, D. S.; Wells, B. O.; Borg, A.; Ellis, W.; Kang, J. S.; Oh, S.-J.; Lindau, I.; Spicer, W. E. Photoemission Study of CoO. *Phys. Rev. B* **1990**, 42, 1817–1828.
- (48) Wi, S. C.; Kang, J.-S.; Kim, J. H.; Cho, S.-B.; Kim, B. J.; Yoon, S.; Suh, B. J.; Han, S. W.; Kim, K. H.; Kim, K. J.; Kim, B. S.; Song, H. J.; Shin, H. J.; Shim, J. H.; Min, B. I. Electronic Structure of $Zn_{1-x}Co_xO$ Using Photoemission and X-Ray Absorption Spectroscopy. *Appl. Phys. Lett.* **2004**, *84*, 4233–4235.
- (49) Quilty, J. W.; Shibata, A.; Son, J.-Y.; Takubo, K.; Mizokawa, T.; Toyosaki, H.; Fukumura, T.; Kawasaki, M. Signature of Carrier-Induced Ferromagnetism in ${\rm Ti}_{1-x}{\rm Co}_x{\rm O}_{2-\delta}$: Exchange Interaction between High-Spin ${\rm Co}^{2+}$ and the Ti 3d Conduction Band. *Phys. Rev. Lett.* **2006**, *96*, 027202.
- (50) Chuang, T. J.; Brundle, C. R.; Rice, D. W. Interpretation of the X-Ray Photoemission Spectra of Cobalt Oxides and Cobalt Oxide Surfaces. *Surf. Sci.* **1976**, *59*, 413–429.
- (51) Langell, M. A.; Anderson, M. D.; Carson, G. A.; Peng, L.; Smith, S. Valence-Band Electronic Structure of Co₃O₄ Epitaxy on CoO(100). *Phys. Rev. B: Condens. Matter Mater. Phys.* **1999**, 59, 4791–4798
- (52) Vagadia, M.; Ravalia, A.; Katba, S.; Solanki, P. S.; Bapna, K.; Kumar, M.; Choudhary, R. J.; Phase, D. M.; Kuberkar, D. G. Co-Substitution Driven Electronic Structure Modifications in $Zn_{1-x}Co_xO$. *J. Alloys Compd.* **2014**, *610*, 113–117.
- (53) Kumar, S.; Basu, S.; Rana, B.; Barman, A.; Chatterjee, S.; Jha, S. N.; Bhattacharyya, D.; Sahoo, N. K.; Ghosh, A. K. Structural, Optical and Magnetic Properties of Sol–gel Derived ZnO:Co Diluted Magnetic Semiconductor Nanocrystals: An EXAFS Study. *J. Mater. Chem. C* 2014, 2 (3), 481–495.
- (54) Singh, J.; Ranwa, S.; Akhtar, J.; Kumar, M. Growth of Residual Stress-Free ZnO Films on SiO 2 /Si Substrate at Room Temperature for MEMS Devices. *AIP Adv.* **2015**, *5* (6), 067140.
- (55) Ashokkumar, M.; Muthukumaran, S. Microstructure, Optical and FTIR Studies of Ni, Cu Co-Doped ZnO Nanoparticles by Co-Precipitation Method. *Opt. Mater. (Amsterdam, Neth.)* **2014**, 37 (C), 671–678.
- (56) Peiteado, M.; Caballero, A. C.; Makovec, D. Thermal Evolution of ZnCo2O4 Spinel Phase in Air. *J. Ceram. Soc. Jpn.* **2010**, *118* (1377), 337–340.
- (57) Butter, E. Chemistry of the Elements; John Wiley & Sons, Ltd.: 1985; Vol. 20.
- (58) Shannon, R. D. Revised Effective Ionic Radii and Systematic Studies of Interatomic Distances in Halides and Chalcogenides. *Acta Crystallogr., Sect. A* **1976**, 32 (5), 751–767.
- (59) Tuan, A. C.; Bryan, J. D.; Pakhomov, A. B.; Shutthanandan, V.; Thevuthasan, S.; McCready, D. E.; Gaspar, D.; Engelhard, M. H.; Rogers, J. W.; Krishnan, K.; Gamelin, D. R.; Chambers, S. A. Epitaxial Growth and Properties of Cobalt-Doped ZnO on α -Al₂O₃ Single-Crystal Substrates. *Phys. Rev. B: Condens. Matter Mater. Phys.* **2004**, 70, 054424.

- (60) Gandhi, V.; Ganesan, R.; Abdulrahman Syedahamed, H. H.; Thaiyan, M. Effect of Cobalt Doping on Structural, Optical, and Magnetic Properties of ZnO Nanoparticles Synthesized by Coprecipitation Method. *J. Phys. Chem. C* **2014**, *118*, 9715–9725.
- (61) Altintas Yildirim, O.; Arslan, H.; Sönmezoğlu, S. Facile Synthesis of Cobalt-Doped Zinc Oxide Thin Films for Highly Efficient Visible Light Photocatalysts. *Appl. Surf. Sci.* **2016**, 390, 111–121.
- (62) Šutka, A.; Käämbre, T.; Pärna, R.; Juhnevica, I.; Maiorov, M.; Joost, U.; Kisand, V. Co Doped ZnO Nanowires as Visible Light Photocatalysts. *Solid State Sci.* **2016**, *56*, 54–62.
- (63) Aljawf, R. N.; Rahman, F.; Kumar, S. Defects/Vacancies Engineering and Ferromagnetic Behavior in Pure ZnO and ZnO Doped with Co Nanoparticles. *Mater. Res. Bull.* **2016**, *83*, 108–115.
- (64) Wang, S.; Li, P.; Liu, H.; Li, J.; Wei, Y. The Structure and Optical Properties of ZnO Nanocrystals Dependence on Co-Doping Levels. J. Alloys Compd. 2010, 505, 362–366.
- (65) Li, P.; Wang, S.; Li, J.; Wei, Y. Structural and Optical Properties of Co-Doped ZnO Nanocrystallites Prepared by a One-Step Solution Route. *J. Lumin.* **2012**, *132*, 220–225.
- (66) Wang, X.; Zheng, R.; Liu, Z.; Ho, H.; Xu, J.; Ringer, S. P. Structural, Optical and Magnetic Properties of Co-Doped ZnO Nanorods with Hidden Secondary Phases. *Nanotechnology* **2008**, *19*, 455702.
- (67) Barnett, C. J.; Smith, N. A.; Jones, D. R.; Maffeis, T. G. G.; Cobley, R. J. Effects of Vacuum Annealing on the Conduction Characteristics of ZnO Nanosheets. *Nanoscale Res. Lett.* **2015**, *10*, 368
- (68) Yu, C.; Qiu, K.-Q.; Chen, Q.-Y. Thermodynamic Analysis of Silicothermic Reduction Zinc Oxide in Vacuum. *Acta Phys.-Chim. Sin.* **2011**, 27 (06), 1312.
- (69) Lim, S.-W.; Hwang, D.-K.; Myoung, J.-M. Observation of Optical Properties Related to Room-Temperature Ferromagnetism in Co-Sputtered $\mathrm{Zn}_{1-x}\mathrm{Co}_x\mathrm{O}$ Thin Films. *Solid State Commun.* **2003**, *125*, 231–235.
- (70) Karzazi, O.; Sekhar, K. C.; El Amiri, A.; Hlil, E. K.; Conde, O.; Levichev, S.; Agostinho Moreira, J.; Chahboun, A.; Almeida, A.; Gomes, M. J. M. Structural, Optical and Magnetic Properties of Pulsed Laser Deposited Co-Doped ZnO Films. *J. Magn. Magn. Mater.* **2015**, 395, 28–33.
- (71) Xu, X.-H.; Qin, X.-F.; Jiang, F.-X.; Li, X.-L.; Chen, Y.; Gehring, G. A. The Dopant Concentration and Annealing Temperature Dependence of Ferromagnetism in Co-Doped ZnO Thin Films. *Appl. Surf. Sci.* **2008**, 254, 4956–4960.
- (72) Park, J. H.; Kim, M. G.; Jang, H. M.; Ryu, S.; Kim, Y. M. Co-Metal Clustering as the Origin of Ferromagnetism in Co-Doped ZnO Thin Films. *Appl. Phys. Lett.* **2004**, *84*, 1338–1340.
- (73) Ip, K.; Frazier, R. M.; Heo, Y. W.; Norton, D. P.; Abernathy, C. R.; Pearton, S. J.; Kelly, J.; Rairigh, R.; Hebard, A. F.; Zavada, J. M.; Wilson, R. G. Ferromagnetism in Mn- and Co-Implanted ZnO Nanorods. J. Vac. Sci. Technol. B Microelectron. J. Vac. Sci. Technol., B: Microelectron. Process. Phenom. 2003, 21, 1476—1481.
- (74) Martín-González, M. S.; Fernández, J. F.; Rubio-Marcos, F.; Lorite, I.; Costa-Krämer, J. L.; Quesada, A.; Bañares, M. A.; Fierro, J. L. G. Insights Into the Room Temperature Magnetism of ZnO/Co3O4Mixtures. *J. Appl. Phys.* **2008**, *103*, 083905.
- (75) Fontaina-Troitino, N.; Liebana-Vinas, S.; Rodriguez-Gonzalez, B.; Li, Z.-A.; Spasova, M.; Farle, M.; Salgueirino, V. Room-Temperature Ferromagnetism in Antiferromagnetic Cobalt Oxide Nanooctahedra. *Nano Lett.* **2014**, *14*, 640–647.
- (76) Cao, Q.; He, S.; Deng, Y.; Zhu, D.; Cui, X.; Liu, G.; Zhang, H.; Yan, S.; Chen, Y.; Mei, L. Raman Scattering Investigations on Co-Doped ZnO Epitaxial Films: Local Vibration Modes and Defect Associated Ferromagnetism. *Curr. Appl. Phys.* **2014**, *14*, 744–748.
- (77) Pemmaraju, C. D.; Hanafin, R.; Archer, T.; Braun, H. B.; Sanvito, S. Impurity-Ion Pair Induced High-Temperature Ferromagnetism in Co-Doped ZnO. *Phys. Rev. B: Condens. Matter Mater. Phys.* **2008**, 78, 054428.